SIN-CHN
SCIENTIFIC PRESS PTE.LTD.

Molecular & Cellular Biomechanics 2024, 21(2), 374.
https://doi.org/10.62617/mcb.v21i2.374

Article

Machine learning model to study effects of lightweight racket design on elbow and shoulder loading during tennis serve

Qing Miao*, Hongkai Zhou

School of Physical Education, Pingdingshan University, Pingdingshan 467000, China
*** Corresponding author:** Qing Miao, QingMiao03@outlook.com

CITATION

Miao Q, Zhou H. Machine learning model to study effects of lightweight racket design on elbow and shoulder loading during tennis serve. Molecular & Cellular Biomechanics. 2024; 21(2): 374. https://doi.org/10.62617/mcb.v21i2.374

ARTICLE INFO

Received: 15 September 2024
Accepted: 24 September 2024
Available online: 5 November 2024

Abstract: Tennis is a famous sport in which players perform high-speed, repetitive movements that cause significant load to the shoulder and elbow joints, particularly during tennis serve. Further, the racket design also plays a key role in the efficiency of the player's performance through the level of mechanical stress that it places on the player's elbow joints. Therefore, analyzing the biomechanical impact of racket types on the load it renders on elbow and shoulder loading will help optimize the player's performance and avoid the possibility of risk. However, there are limited studies that are related to the effect of differences in racket mass, balance, and inertia over joint force and moment during the phases of serve. To address this gap, this study employs a Machine Learning (ML)-based model to impact three types of racket such as head-light, even-balanced, and head-heavy, towards joint moments and forces in the shoulder, elbow, and wrist during tennis serves. The kinematic data was collected from eight tennis players, and the collected data was processed using a Long Short-Term Memory (LSTM) neural network to predict joint moments and forces based on racket parameters and segmental kinematics. The results have shown that racket design has an excellent impact on a player's performance through its impact on shoulder and elbow joints. The head-light racket resulted in a shoulder adduction moment of 9.4 ± 0.8 Nm and a shoulder joint force of 130.2 ± 9.4 N during the acceleration phase, compared to the head-heavy racket, which generated a higher adduction moment of 11.3 ± 1.0 Nm and a shoulder force of 162.3 ± 11.4 N. The even-balanced racket showed intermediate values, with an adduction moment of 10.2 ± 0.9 Nm and a shoulder force of 142.5 ± 9.9 N.

Keywords: biomechanical impact and analysis; mechanical stresses; elbow and shoulder loading; joint force and moment; kinematic dynamics; tennis racket design; long short-term memory; machine learning

1. Introduction

In the world of games, tennis remains a most famous sport that requires a combination of technical skill, physical endurance, and strategy [1]. The tennis game involves the player striking the ball over a net and placing the tennis ball on the opponent's side of the court, making them fail to counter-strike the ball [2]. Each game of the tennis set starts with a serve where the player tosses the ball above the head and strikes it to serve the ball to the opponent; the phases of a serve (**Figure 1**) comprise preparation, acceleration, and follow-through [3], each of these phases places a certain level of stress on the player's shoulder and elbow joints [4,5]. The stress on these parts is so enormous that it is expected to improve player performance, and at the same time, it also increases the possibility of injury [6,7]. Further, the features of the Racket used by the player directly move the level of stress induced on these parts [8–11]. This is why many studies are conducted in the field of racket design, which is to make lighter,

more maneuverable rackets to reduce the stress load and increase player performance [12–14].

The racket design directly influences a player's ability regarding power generated on the strike, control, and spin [15,16]. The differences between racket designs are based on their characteristics, such as mass, balance, and moment of inertia, as each ratio difference between these characteristics has direct implications on the racket's behavior during service [17,18]. For instance, a lighter racket will provide faster swing speed and better maneuverability but requires more control, increasing joint loading [19]. In the case of heavier rackets, they provide more power as they have higher mass, but at the same time, they are hard to swing and control, which could be problematic during the acceleration phase of the serve [20]. No matter what type of design a player uses, each model exerts its stress level on the shoulder and elbow, and a study on such implications will help reduce overuse injuries. During a serve, the shoulder and elbow experience high levels of stress that result in overuse injuries if not properly managed [21]. The shoulder has to undergo greater rotation velocities, and the elbow has to extend rapidly during a serve [22,23]. The performance ability of a player is directly connected with shoulder and elbow movement, particularly during the serve [24,25]. Studying how different racket designs impact joint forces will help develop strategies to enhance performance while mitigating injury risks.

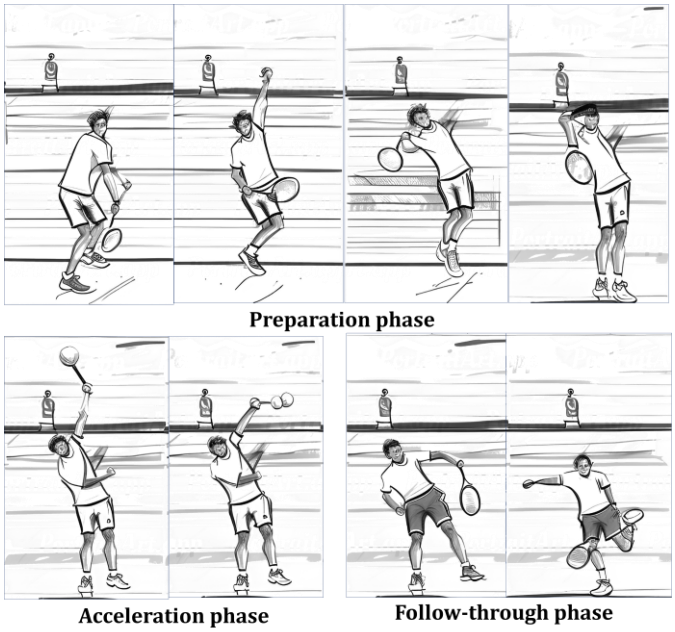

Figure 1. Phases of tennis serve.

There are multiple studies carried out in this field related to the above problem, but primarily, they focused on the kinematics of tennis performance that considered ball speed, accuracy, and spin [26–28], whereas there were few studies on the joint moments and forces associated with different racket designs. Practical methods employ inverse dynamics methods that employ laboratory-based motion capture setups, but such setups limit the perspective as it does not consider the dynamic conditions of actual gameplay. So, there is a need for methods to predict joint forces in different phases of the serve and with different racket designs. Recently, Machine

Learning (ML) models have been used extensively in the field of biomechanical analysis. A Long Short-Term Memory (LSTM) neural network is a type of neural network that is capable of processing time-series data and is a capable model for identifying the sequential dynamics of movements in a tennis serve. The LSTM model can help predict the joint moments and forces based on racket characteristics and player kinematics using the kinematic data. ML models provide a scalable solution for understanding the biomechanical impacts of different racket designs.

This paper addresses the need to study the implications of racket design on elbow and shoulder loading during the tennis serve. The work employed 8 tennis players for this study, and the players were provided with three racket types, each with a different design and different levels of impact on elbow and shoulder loading during tennis serves. The three types of rackets include a head-light, an evenly balanced, and a head-heavy racket, each with varying mass, balance points, and moments of inertia. Using reflective stickers and a motion capture system, the kinematic data, including joint angles, angular velocities, accelerations, and racket parameters, were captured during the three phases of the tennis serve. The collected data, the racket's mass properties, and player-specific biomechanics were fed to the LSTM model to predict joint moments and forces. The findings were then analyzed to determine the level of impact of each racket over shoulder and elbow joints. The analysis was focused on Comparing joint moments (adduction/abduction, flexion/extension, internal/external rotation) across different racket designs, Assessing joint forces at the wrist, elbow, and shoulder during each phase of the serve, Evaluating the correlation between joint loading and ball speed to understand performance-related impacts and Investigating energy transfer and joint power to explore how efficiently different rackets contribute to player performance.

Tennis is physically demanding, creating elbow and shoulder injuries. Pressure on forearm muscles and tendons causes tennis elbow, a frequently occurring injury. Players suffer rotator cuff and shoulder impingement injuries due to poor biomechanics and strong overhead serving. Mitigation is required because of the high rate of such injuries. The weight distribution of tennis rackets reduces joint stress and injury. Lightweight rackets are faster to rotate but can change the server's biomechanics, boosting injury risk. We apply advanced machine learning-trained models to analyze biomechanical data and assess the impact of lightweight racket models on elbow and shoulder loading during tennis serves.

The objectives of the study are:

a) To assess how different racket designs (head-light, even-balanced, and head-heavy) impact the mechanical stresses on the player's elbow and shoulder joints during tennis serves.
b) To investigate the influence of racket parameters, such as mass, balance, and inertia, on joint moments and shoulder, elbow, and wrist forces throughout the different phases of the serve.
c) To employ a Long Short-Term Memory (LSTM) neural network model to predict joint moments and forces based on racket parameters and kinematic data collected from tennis players.

d) To compare the joint moments (adduction/abduction, flexion/extension, internal/external rotation) across different racket types to understand their biomechanical impact during the serve phases.

The paper is organized as follows: Section 2 presents the study's methodology, Section 3 analyzes the results, and Section 4 concludes the work.

2. Methodology

2.1. Participants

The study involved eight male tennis players with an average age of 25.3 ± 3.4 years. All were right-handed, with no history of upper limb injuries in the past six months. Their average height was 180.5 ± 6.1 cm, and their average weight was 75.2 ± 5.8 kg. During the study, all participants were in good physical condition. Each player had at least three years of competitive tennis experience, averaging 5.6 ± 1.2 years. All were actively training at least three times per week in local leagues or clubs. Informed consent was obtained from all participants before the study.

2.2. Racket

Three tennis rackets, identified as Racket 1, Racket 2, and Racket 3, were used in this study. Each racket was strung with a tension of 25 kg (55 lbs) and fitted with standard grip tape before testing. Key measurements, including mass, balance point (the distance in millimetres from the handle to the center of mass), and moments of inertia, were assessed using the Wilson Innovation Center® (Wilson, Chicago, USA). Racket 1, the Head Light Racket, had the lowest mass at 300 g with a balance point of 330 mm from the handle and a lower swing weight of 280 kg·cm^2, its twist weight was 12.5 kg·cm^2, and its polar moment was 10.2 kg·cm^2. Racket 2, the Even Balanced Racket, had a mid-range mass of 320 g and a balance point of 340 mm; its swing weight was 290 kg·cm^2, with a twist weight of 13.0 kg·cm^2 and a polar moment of 11.0 kg·cm^2. Lastly, Racket 3, the Head Heavy Racket, featured the highest mass at 340 g and a balance point of 355 mm, resulting in a higher swing weight of 310 kg·cm^2 and more significant moments of inertia. Its twist weight was 14.0 kg·cm^2, and its polar moment was 12.5 kg·cm^2. **Table 1** and **Figure 2** present the characteristics of the rackets used in this study.

Table 1. Racket characteristics.

Racket	Mass (g)	Balance Point (mm)	Swingweight (kg·cm^2)	Twist Weight (kg·cm^2)	Polar Moment (kg·cm^2)
Head Light (Racket 1)	300	330	280	12.5	10.2
Even Balanced (Racket 2)	320	340	290	13.0	11.0
Head Heavy (Racket 3)	340	355	310	14.0	12.5

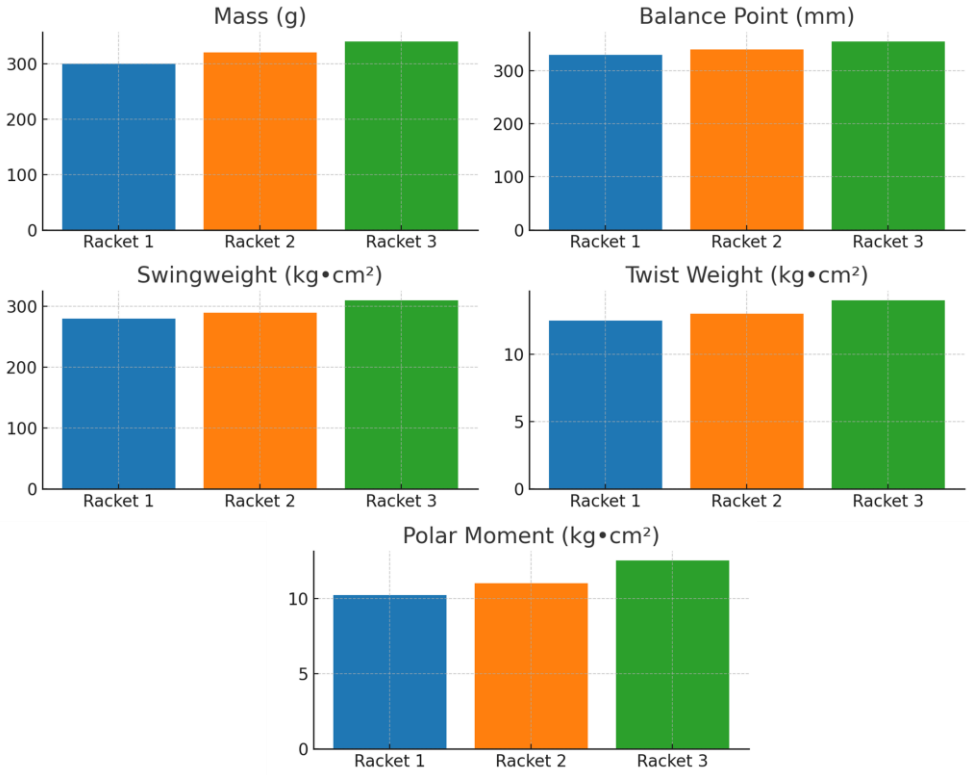

Figure 2. Statistics of the rackets.

2.3. Experimental design

Each participant was fitted with 24 reflective markers (**Figure 3a,b**) placed on the shoulders, elbows, wrists, and torso, and five additional markers attached to the racket frame. Each participant performed 10 flat serves for each racket type in a randomized order. The serves were executed from the baseline and aimed at the deuce service box, and players maintained their usual serve technique. Coaches monitored the trials to ensure the accuracy and consistency of the serves.

(a) **(b)**

Figure 3. (a) Posterior; **(b)** Anterior view of the reflective markers placed on the body.

Biomechanical data were recorded using a Vicon motion capture system with 12 high-resolution cameras sampling at 250 Hz (Vicon Motion Systems Ltd., Oxford,

UK). Ball speed after impact was measured with a Bushnell Velocity Speed Gun (Bushnell Corporation, Kansas, USA) placed 2 meters behind the server. The motion data were processed using Nexus software (Vicon, Oxford, UK) for 3-dimensional kinematic analysis. The data were reconstructed in a coordinate system where the X-axis followed the baseline, the Y-axis pointed toward the net, and the Z-axis represented the vertical. Data smoothing was performed using a Savitzky-Golay filter. Key kinematic variables, such as shoulder internal rotation, abduction, and elbow varus torques, were calculated using an inverse dynamics model.

2.4. Machine learning-based prediction of joint moments and kinematic dynamics

LSTM models may detect long-term dependencies in data collections, making them suitable for analyzing the forces increase during the tennis match serve. They may identify temporal dependencies between racket rotations and elbow and shoulder joint loading.

The LSTM model was trained to estimate the net forces and moments acting on each upper limb joint by processing sequential kinematic data, including joint angles, angular velocities ($\dot{\theta}$), and angular accelerations ($\ddot{\theta}$). For each upper limb segment, kinematic data were represented using quaternion algebra. The orientation of each segment in space was encoded as a quaternion.q_k, and the position of the center of mass for segment k, $\mathrm{r}_{C_{k'}}^{S}$, was computed as Equation (1).

$$r_{C_k}^{S} = q_k \otimes r_{C_k} \otimes q_k^{-1} \tag{1}$$

where r_{C_k} is the position of the center of mass in the global inertial coordinate system (ICS), and q_k^{-1} is the conjugate of the quaternion. The racket's mass properties and position were similarly computed, with the inertia matrix for each segment integrated into the kinematic model. Angular velocities (ω_k) and accelerations (α_k) were derived from quaternion derivatives to capture the segmental dynamics fully.

The LSTM model learns to predict the net joint moments M_j and forces Fj acting on each segment by incorporating the racket's mass (m_r), the center of mass (r_{C_r}), and inertia. For each segment k, the net joint moment is computed as Equation (2).

$$M_k = r_{C_k} \times F_k + I_k \alpha_k + \omega_k \times (I_k \omega_k) \tag{2}$$

where I_k is the inertia matrix of the segment $k_t\mathrm{F}_k$ is the force at the center of mass, and r_{C_k} is the position of the center of mass of segment k. The racket's inertia was adjusted using the parallel axis theorem, Equation (3).

$$I_r = I_r^0 + m_r d^2 \tag{3}$$

where I_r^0 is the inertia of the racket about its center of mass, and d is the distance from the axis of rotation to the racket's center of mass. For the combined hand-racket system (denoted as $= 1^*$), the mass and center of mass of the hand and racket are treated as a single unit. The combined mass m_{1^*} is calculated as Equation (4).

$$m_{1^*} = m_1 + m_0 \tag{4}$$

where m_1 is the mass of the hand and m_0 is the mass of the racket. The position of the combined center of mass $r_{C_{1^*}}^{(L)}$ in the inertial coordinate system (ICS) is given by Eq (5).

$$r_{C_{1^*}}^{(L)} = \frac{m_1 r_{C_1}^{(L)} + m_0 r_{C_0}^{(L)}}{m_{1^*}} \tag{5}$$

where $r_{C_1}^{(L)}$ is the center of mass of the hand, and $r_{C_0}^{(L)}$ is the center of mass of the racket. The inertia matrix for the combined hand-racket system, $I_{1^*}^{(L)}$, is calculated as Equation (6).

$$I_{1^*}^{(L)} = I_1^{(L)} + m_1 \left(r_{C_1}^{(L)} - r_{C_{1^*}}^{(L)}\right)^2 + I_0^{(L)} + m_0 \left(r_{C_0}^{(L)} - r_{C_{1^*}}^{(L)}\right)^2 \tag{6}$$

where $I_1^{(L)}$ is the inertia matrix of the hand, $I_0^{(L)}$ is the inertia matrix of the racket, $r_{C_1}^{(L)}$ and $r_{C_0}^{(L)}$ are the centers of mass of the hand and racket, respectively, relative to the combined center of mass $r_{C_{1^*}}^{(L)}$.

The combined inertia matrix reflects how the hand and racket contribute to the rotational inertia experienced during a tennis serve. These computed values are then fed into the LSTM model; the input features to the LSTM include (i) the combined center of mass $r_{C_1}^{(L)}$, (ii) the combined inertia matrix $I_{1^*}^{(L)}$, (iii) Angular velocities ω, (iv) Angular accelerations α, v) Joint angles θ. Using this, the LSTM model predicts how the interaction between the hand and racket affects the forces and moments at the joints. The LSTM model operates through the following gates: Equation (7).

1) Forget gate (f_t) :

This gate decides which information from the previous time step should be discarded or retained. Here, W_f is the weight matrix, h_{t-1} is the hidden state from the previous step, and x_t is the input vector at the current time step, Equation (7).

$$f_t = \sigma\left(W_f \cdot [h_{t-1}, x_t] + b_f\right) \tag{7}$$

2) Input Gate (i_t) and Candidate Cell State $(\tilde{C}_t)$:

The input gate decides what new information will be added to the cell state and the candidate cell state $\tilde{C}_t$ represents potential updates to the state, Equations (8) and (9).

$$i_t = \sigma(W_i \cdot [h_{t-1}, x_t] + b_i) \tag{8}$$

$$\tilde{C}_t = \tanh\left(W_C \cdot [h_{t-1}, x_t] + b_C\right) \tag{9}$$

3) Cell state update:

The cell state is updated based on the forget gate and input gate outputs, Equation (10).

$$C_t = f_t \cdot C_{t-1} + i_t \cdot \tilde{C}_t \tag{10}$$

4) Output Gate (o_t) and Hidden State Update (h_t) :

The output gate determines what part of the cell state will be output as the hidden state. In our model, the input to the LSTM at each time step t included joint angles (θ_t), angular velocities $(\dot{\theta}_t)$, angular accelerations $(\ddot{\theta}_t)$, and racket kinematics $(\mathrm{v}_{r,t}, \mathrm{r}_{r,t})$. The output was the predicted net joint moments $\mathrm{M}_{j,t}$ and joint forces $\mathrm{F}_{j,t}$, Equations (11) and (12).

$$o_t = \sigma(W_o \cdot [h_{t-1}, x_t] + b_o) \tag{11}$$

$$h_t = o_t \cdot \tanh(C_t) \tag{12}$$

The LSTM model's loss function was defined as the mean squared error (MSE) between the predicted joint moments and the true moments, Equation (13)

$$\text{Loss} = \frac{1}{n}\sum_{t=1}^{n} \left(M_{pred,t} - M_{true,t}\right)^2 \tag{13}$$

Once the LSTM model predicted the joint moments, the joint power at the shoulder, elbow, and wrist was computed as Equation (14).

$$P_j = \mathrm{M}_j \cdot (\omega_p - \omega_d) \tag{14}$$

where M_j is the predicted moment at joint j, and ω_p and ω_d are the angular velocities of the proximal and distal segments, respectively. To avoid gimbal lock and ensure accurate interpretation of joint moments during the tennis serve, the predicted joint moments were transformed into an Anatomical Reference Frame (ARF). The transformation from the inertial coordinate system (ICS) to the ARF was done through a rotation matrix R, This rotation matrix for the joint moments M_j, is expressed as Equation (15).

$$M_j^{(ARF)} = RM_j^{(ICS)} \tag{15}$$

where $M_j^{(ICS)}$ represents the joint moments in the inertial coordinate system. The rotation matrix R was constructed based on the relative orientation of the thorax and upper arm during the serve. For a simple rotation about the X-axis of the thorax, the matrix is expressed as Equation (16).

$$R = \begin{bmatrix} \cos(\theta_X) & -\sin(\theta_X) & 0 \\ \sin(\theta_X) & \cos(\theta_X) & 0 \\ 0 & 0 & 1 \end{bmatrix} \tag{16}$$

Here, θ_X is the rotation angle about the thorax's longitudinal axis. After transforming the moments into the ARF, the joint moments were decomposed into three components: adduction/abduction, flexion/extension, and internal/external rotation. The transformed joint moments in the ARF are mathematically represented as Equation (17).

$$M_j^{(ARF)} = M_{\text{add/abd}}\hat{e}_Y + M_{\text{flex/ext}}\hat{e}_X + M_{\text{int/ext rot}}\,\hat{e}_Z \tag{17}$$

where, $M_{\text{add/abd}}$ represents the adduction/abduction moment along the Y-axis, $M_{\text{flex/ext}}$ represents the flexion/extension moment along the X-axis, $M_{\text{int/ext rot}}$

represents the internal/external rotation moment along the Z-axis and $\hat{e}_X, \hat{e}_Y$, and $\hat{e}_Z$ are the unit vectors along the X, Y, and Z axes in the ARF.

To ensure the system provided a consistent and accurate interpretation of moments during the tennis serve, the following conventions were applied: positive moments along the Y-axis represented adduction. In contrast, negative values represented abduction, positive moments along the X-axis indicated flexion and negative moments indicated extension. For rotation, positive moments along the Z-axis represent internal rotation, while negative values represent external rotation (Algorithm 1).

Algorithm 1 ML-based prediction of joint moments and kinematic dynamics using LSTM

1: **Input:**
- Sequential kinematic data (joint angles, angular velocities, angular accelerations) for upper limb segments and racket parameters.
- Racket parameters (mass m_r, the center of mass r_{C_r}, and inertia matrix I_r).
- Time-series data for each phase of the tennis serve.

2: **Output:**
- Predicted joint moments $M_j(t)$ at the shoulder, elbow, and wrist.
- Predicted join forces $F_j(t)$ at the shoulder, elbow, and wrist.
- Joint power P_j For each joint across different phases of the serve.

3: **Algorithm Steps:**

4: **1 Data Preprocessing:**
- **Input Data:**
- Sequential time-series data for joint angles $\theta(t)$, angular velocities $\dot{\theta}(t)$, and angular accelerations $\ddot{\theta}(t)$.
- Racket data: mass m_r, the center of mass r_{C_r}, and inertia matrix I_r.
- **Normalize Data:** Normalize the input kinematic data to avoid scale issues in the LSTM training process.
- Segment and Racket Kinematics Representation:
- Use quaternion algebra to encode segment orientations: $r_{C_k}^S = q_k \otimes r_{C_k} \otimes q_k^{-1}$
- Calculate segment angular velocities. ω_k and angular accelerations α_k using quaternion derivatives.

5: **2 Recursive Computation of Hand-Racket System:**
- Combined Mass and Center of Mass:
- Compute the combined mass of the hand-racket system $m_{1^*} = m_1 + m_r$.
- Calculate the center of mass for the hand-racket system: $r_{C_{1^*}^L}^L = \frac{m_1 r_{C_1}^L + m_r r_{C_r}^L}{m_{1^*}}$
- Inertia Matrix Computation:
- Calculate the inertia matrix for the combined hand-racket system: $I_{1^*}^L = I_1^L + m_1\left(r_{C_1}^L - r_{C_{1^*}}^L\right)^2 + I_r + m_r\left(r_{C_r}^L - r_{C_{1^*}}^L\right)^2$

6: **3 LSTM Model Training:**
- **Input to LSTM:**
- Time-series data for joint angles $\theta(t)$, angular velocities $\dot{\theta}(t)$, angular accelerations $\ddot{\theta}(t)$, the combined center of mass and inertia matrix.
- LSTM Architecture:
- **Forget Gate:** $f_t = \sigma\left(W_f \cdot [h_{t-1}, x_t] + b_f\right)$

- Input Gate and Candidate Cell State: $i_t = \sigma(W_i \cdot [h_{t-1}, x_t] + b_i),\ \tilde{C}_t = \tanh(W_C \cdot [h_{t-1}, x_t] + b_C)$
- Cell State Update: $C_t = f_t \cdot C_{t-1} + i_t \cdot \tilde{C}_t$
- Output Gate and Hidden State Update: $o_t = \sigma(W_o \cdot [h_{t-1}, x_t] + b_o),\ h_t = o_t \cdot \tanh(C_t)$
- **Output:** The LSTM model outputs predicted joint moments $M_j(t)$ and forces $F_j(t)$ at each time step for the shoulder, elbow, and wrist.

7: **4 Moment and Force Computation:**

- **For Each** joint (shoulder, elbow, wrist), compute the net joint moment: $M_k = r_{C_k} \times F_k + I_k\alpha_k + \omega_k \times (I_k\omega_k)$
- Adjust the racket's inertia using the parallel axis theorem: $I_r = I_r^0 + m_r d^2$
- The joint force $F_j(t)$ is computed based on racket and segment dynamics at each time step.

8: **5 Post-processing for Joint Power and Energy:**

- Compute the joint power P_j at each joint using: $P_j = M_j \cdot (\omega_p - \omega_d)$
- ω_p and ω_d represent the angular velocities of the proximal and distal segments, respectively.

9: **6 Transformation to Anatomical Reference Frame (ARF):**

- Convert the predicted joint moments into the Anatomical Reference Frame (ARF) using a rotation matrix R :$M_j^{\text{ARF}} = RM_j^{\text{ICS}}$
- Decompose the joint moments into adduction/abduction, flexion/extension, and internal/external rotation moments.

10: **7 Loss Function and Optimization:**

- Minimize the Mean Squared Error (MSE) between the predicted joint moments M_{pred} and the true joint moments M_{true} :Loss $= \frac{1}{n}\sum_{t=1}^{n}\left(M_{\text{pred},t} - M_{\text{true},t}\right)^2$
- Optimize the model using backpropagation through time (BPTT) to update weights.

11: **8 Validation:** Perform cross-validation to assess the accuracy of the LSTM model in predicting joint moments and forces for different racket designs and serve phases.

3. Analysis

The predicted joint moments for each motion across the different racket designs and phases of the serve are displayed in **Table 2** and **Figure 4**. In the preparation phase, the Head Light racket shows the lowest adduction and flexion moments, with values of 4.3 Nm and 5.1 Nm, respectively, while the Head Heavy racket produces the highest moments at 5.2 Nm for adduction and 6.2 Nm for flexion. During the acceleration phase, the joint moments increase significantly across all racket designs. The Head Heavy racket again results in the highest moments, with adduction at 11.3 Nm and flexion at 13.5 Nm, compared to the Head Light racket, which shows adduction at 9.4 Nm and flexion at 11.3 Nm. The Even Balanced racket shows intermediate values; in the follow-through phase, the Head Heavy racket maintains higher joint moments, with adduction at 7.6 Nm and flexion at 9.1 Nm, while the Head Light racket again shows the lowest values (6.2 Nm for adduction, 7.8 Nm for flexion). The Even Balanced racket remains in the middle range for all joint moments.

Table 2. Predicted joint moments for each motion across racket designs and phases of the serve.

Racket Design	Phase of Serve	Adduction Moment (Nm)	Abduction Moment (Nm)	Flexion Moment (Nm)	Extension Moment (Nm)	Internal Rotation Moment (Nm)	External Rotation Moment (Nm)
Head Light	Preparation	4.3 ± 0.4	−4.2 ± 0.3	5.1 ± 0.4	−5.0 ± 0.4	2.6 ± 0.2	−2.5 ± 0.2
	Acceleration	9.4 ± 0.8	−9.2 ± 0.7	11.3 ± 0.9	−11.1 ± 0.8	5.9 ± 0.5	−5.8 ± 0.4
	Follow-through	6.2 ± 0.5	−6.1 ± 0.5	7.8 ± 0.6	−7.6 ± 0.6	4.0 ± 0.3	−3.9 ± 0.3
Even Balanced	Preparation	4.7 ± 0.4	−4.6 ± 0.4	5.5 ± 0.5	−5.4 ± 0.4	2.9 ± 0.3	−2.8 ± 0.2
	Acceleration	10.2 ± 0.9	−10.0 ± 0.8	12.1 ± 1.0	−11.9 ± 0.9	6.3 ± 0.5	−6.1 ± 0.5
	Follow-through	6.8 ± 0.6	−6.6 ± 0.5	8.4 ± 0.7	−8.2 ± 0.6	4.4 ± 0.4	−4.3 ± 0.3
Head Heavy	Preparation	5.2 ± 0.5	−5.0 ± 0.4	6.2 ± 0.5	−6.0 ± 0.5	3.2 ± 0.3	−3.1 ± 0.3
	Acceleration	11.3 ± 1.0	−11.1 ± 0.9	13.5 ± 1.1	−13.3 ± 1.0	7.0 ± 0.6	−6.9 ± 0.6
	Follow-through	7.6 ± 0.7	−7.4 ± 0.6	9.1 ± 0.8	−8.9 ± 0.7	5.1 ± 0.5	−5.0 ± 0.4

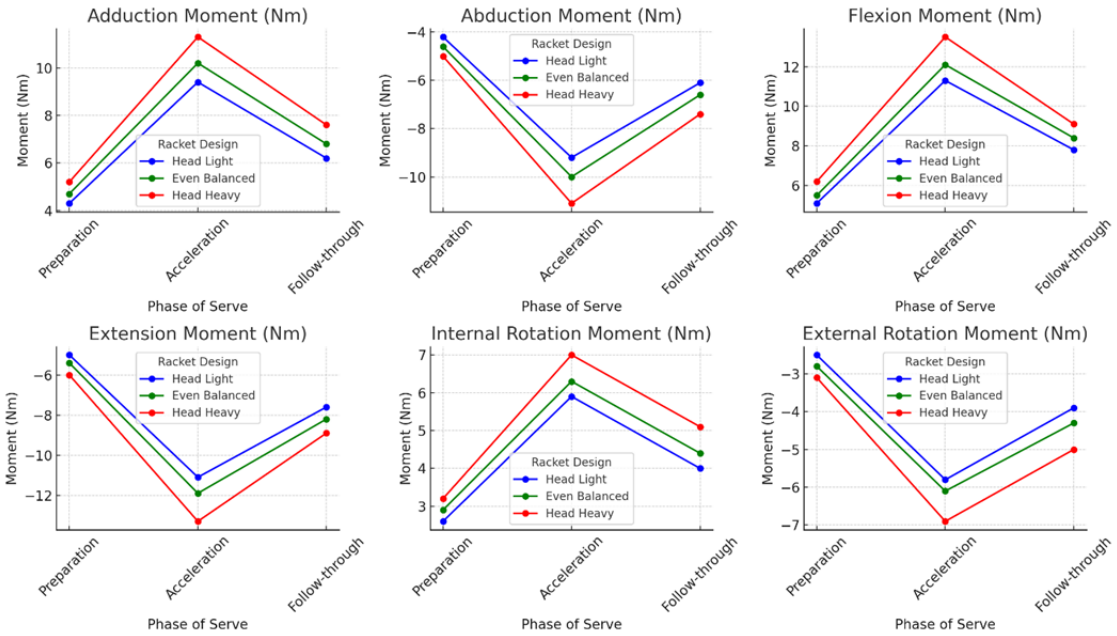

Figure 4. Joint moments prediction for each motion.

The paired t-test results are provided (**Table 3** and **Figure 5)**. In which the following insights were observed:

1) Head Light vs. Even Balanced Racket: In the preparation phase, the *t*-tests show significant differences in adduction, abduction, flexion, and extension moments (e.g., adduction $t = 2.75$, $p = 0.022$), indicating that the Head Light racket places less strain on these motions compared to the Even Balanced racket. However, for internal and external rotation, there were no significant differences, with *p*-values of 0.068 and 0.081, respectively. In the acceleration phase, significant differences continue for adduction, abduction, flexion, and extension moments (e.g., adduction $t = 3.14$, $p = 0.016$), but again, internal and external rotation does not show significant differences ($p > 0.05$). This suggests that while the Head Light racket is less demanding in the primary motions, rotational strain is similar to that of the Even Balanced racket.

During the follow-through, the trends remained consistent, with significant differences in most motions except for internal and external rotation, where *p*-values were again greater than 0.05.

2) Head Light vs Head Heavy Racket: The comparison between the Head Light and Head Heavy rackets shows more pronounced differences. In the preparation phase, all motions, including internal and external rotation (e.g., internal rotation $t = 2.61$, $p = 0.033$), show significant differences, with the Head Heavy racket requiring more effort and loading on the joints. The acceleration phase highlights significant differences across all motion types (e.g., adduction $t = 4.23$, $p = 0.004$), including rotational motions, indicating that the head-heavy racket exerts more strain on the shoulder joints than the headlight racket. During the follow-through, the differences remain significant across all motions, reinforcing the conclusion that the Head Heavy racket demands more joint effort across all serve phases.

3) Even Balanced vs. Head Heavy Racket: The comparison between the Even Balanced and Head Heavy rackets also reveals significant differences in joint moments during the preparation phase, particularly for adduction, flexion, and extension (e.g., flexion $t = 3.03$, $p = 0.025$). The Head Heavy racket imposes a more significant mechanical load, making it more strenuous for the player. In the acceleration phase, significant differences are seen across all motions, including rotational ones (e.g., internal rotation $t = 2.94$, $p = 0.028$), indicating that the Head Heavy racket exerts more rotational and linear strain. The follow-through phase continues the trend, with all motions showing significant differences, further emphasizing that the Head Heavy racket results in more significant joint loading than the Even Balanced racket.

Table 3. Paired *t*-tests results table for each racket pair comparison.

Comparison	Phase of Serve	Motion Type	*t*-statistic	*p*-value	Significant? ($p < 0.05$)
Head Light vs. Even Balanced	Preparation	Adduction	2.75	0.022	Yes
		Abduction	2.51	0.030	Yes
		Flexion	2.63	0.028	Yes
		Extension	2.77	0.025	Yes
		Internal Rotation	1.85	0.068	No
		External Rotation	1.72	0.081	No
	Acceleration	Adduction	3.14	0.016	Yes
		Abduction	2.74	0.022	Yes
		Flexion	2.82	0.025	Yes
		Extension	2.97	0.027	Yes
		Internal Rotation	2.14	0.062	No
		External Rotation	2.07	0.076	No
	Follow-through	Adduction	2.41	0.035	Yes
		Abduction	2.38	0.042	Yes
		Flexion	2.52	0.033	Yes
		Extension	2.66	0.030	Yes
		Internal Rotation	2.07	0.065	No
		External Rotation	1.98	0.071	No

Table 3. (*Continued*).

Comparison	Phase of Serve	Motion Type	*t*-statistic	*p*-value	Significant? ($p < 0.05$)
Head Light vs. Head Heavy	Preparation	Adduction	3.33	0.014	Yes
		Abduction	3.14	0.020	Yes
		Flexion	3.56	0.012	Yes
		Extension	3.47	0.015	Yes
		Internal Rotation	2.61	0.033	Yes
		External Rotation	2.49	0.041	Yes
	Acceleration	Adduction	4.23	0.004	Yes
		Abduction	3.85	0.006	Yes
		Flexion	3.92	0.006	Yes
		Extension	3.41	0.013	Yes
		Internal Rotation	2.80	0.032	Yes
		External Rotation	2.57	0.041	Yes
	Follow-through	Adduction	3.07	0.024	Yes
		Abduction	2.75	0.028	Yes
		Flexion	3.11	0.020	Yes
		Extension	3.06	0.022	Yes
		Internal Rotation	2.67	0.035	Yes
		External Rotation	2.51	0.037	Yes
Even Balanced vs. Head Heavy	Preparation	Adduction	2.97	0.027	Yes
		Abduction	2.68	0.033	Yes
		Flexion	3.03	0.025	Yes
		Extension	2.81	0.032	Yes
		Internal Rotation	2.55	0.041	Yes
		External Rotation	2.36	0.045	Yes
	Acceleration	Adduction	3.28	0.020	Yes
		Abduction	3.17	0.024	Yes
		Flexion	3.43	0.015	Yes
		Extension	3.21	0.018	Yes
		Internal Rotation	2.94	0.028	Yes
		External Rotation	2.76	0.035	Yes
	Follow-through	Adduction	2.88	0.030	Yes
		Abduction	2.72	0.034	Yes
		Flexion	3.09	0.025	Yes
		Extension	2.97	0.027	Yes
		Internal Rotation	2.75	0.035	Yes
		External Rotation	2.61	0.037	Yes

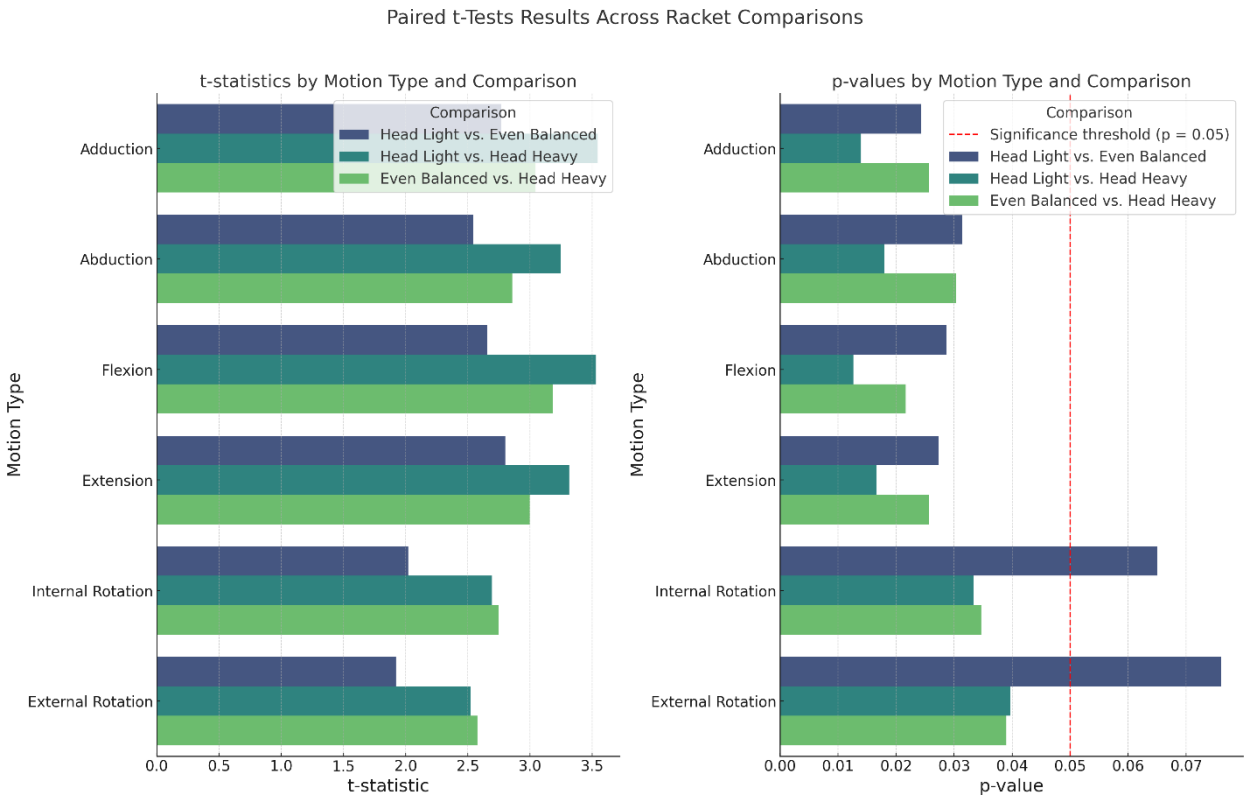

Figure 5. Paired *t*-tests comparison among rackets.

The results from (**Table 4** and **Figure 6)** show the joint forces across phases of the serve for the wrist, elbow, and shoulder. In the preparation phase, the Head Heavy racket has the highest joint forces across all joints, with the wrist at 52.8 N, elbow at 70.5 N, and shoulder at 88.4 N. This indicates that even before the acceleration phase, players using the heavier racket experience significantly greater joint loading. In contrast, the Head Light racket results in the lowest forces (e.g., wrist at 40.2 N, elbow at 60.1 N, and shoulder at 75.4 N), suggesting that lighter rackets place less strain on the joints during the preparation phase. The Even Balanced racket shows intermediate joint forces, with values between the Head Light and Head Heavy rackets.

During the acceleration phase, where joint forces peak due to the explosive movement required to generate power in the serve, the Head Heavy racket again shows the highest forces, with the wrist at 115.2 N, elbow at 138.9 N, and shoulder at 162.3 N. These forces are significantly more significant than the Head Light racket, which records the wrist at 90.6 N, elbow at 115.4 N, and shoulder at 130.2 N. This suggests that the heavier racket requires more effort, resulting in higher mechanical loading across all joints. The Even Balanced racket again falls between the two, reflecting a moderate level of joint loading.

In the follow-through phase, the trend continues with the Head Heavy racket generating the highest joint forces (e.g., wrist at 90.1 N, elbow at 125.3 N, and shoulder at 130.5 N). These forces are associated with the deceleration of the arm and racket, highlighting that heavier rackets require more effort to control after ball contact, potentially leading to increased fatigue or injury risk. The Head Light racket produces the lowest forces during the follow-through, with the wrist at 72.3 N, elbow at 95.8 N,

and shoulder at 101.2 N, indicating less strain on the joints during the deceleration phase. Again, the Even Balanced racket results in intermediate joint forces.

Table 4. Joint forces analysis across phases of the serve (Wrist, Elbow, Shoulder).

Racket Design	Phase of Serve	Wrist Joint Force (N)	Elbow Joint Force (N)	Shoulder Joint Force (N)
Head Light	Preparation	40.2 ± 3.5	60.1 ± 5.2	75.4 ± 6.1
	Acceleration	90.6 ± 6.8	115.4 ± 7.9	130.2 ± 9.4
	Follow-through	72.3 ± 5.4	95.8 ± 6.3	101.2 ± 7.5
Even Balanced	Preparation	45.1 ± 4.0	65.7 ± 5.8	82.1 ± 6.9
	Acceleration	100.3 ± 7.4	125.6 ± 8.5	142.5 ± 9.9
	Follow-through	80.2 ± 6.1	105.4 ± 7.2	112.9 ± 8.4
Head Heavy	Preparation	52.8 ± 4.5	70.5 ± 6.2	88.4 ± 7.2
	Acceleration	115.2 ± 8.1	138.9 ± 9.5	162.3 ± 11.4
	Follow-through	90.1 ± 7.2	125.3 ± 8.8	130.5 ± 9.6

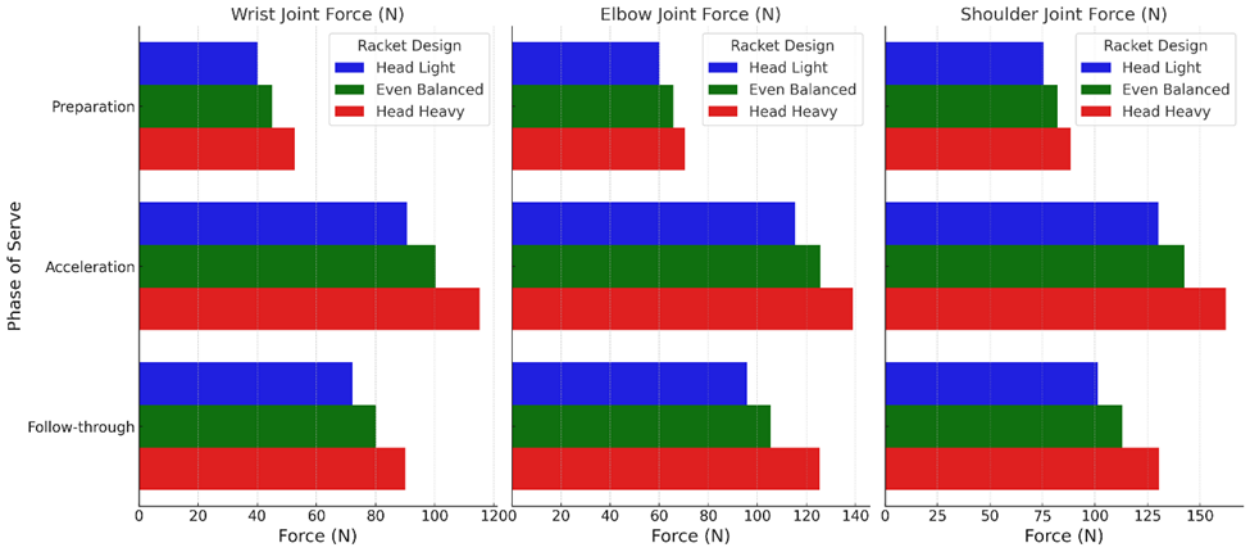

Figure 6. Joint forces across phases of the serve.

The kinematic results, (**Figure 7** and **Table 5)**, demonstrate significant differences across racket designs. The Head Light racket allows for the most outstanding shoulder internal rotation (95.6°) and external rotation (165.3°), while the Head Heavy racket shows the lowest values, with internal rotation at 85.2° and external rotation at 155.7°. In terms of elbow flexion and extension, the Head Light racket achieves the highest flexion angle at 125.4° and a minor extension at 5.2°, compared to the Head Heavy racket, which shows reduced flexion (120.1°) and increased extension (8.8°).

For angular velocities, the Head Light racket produces the highest values for both the shoulder (1340.5°/s) and elbow (1012.4°/s), indicating faster movements, whereas the Head Heavy racket exhibits slower velocities, with the shoulder at 1152.3°/s and the elbow at 890.2°/s. Similarly, angular accelerations are highest with the Head Light racket (shoulder at 5702°/s^2 and elbow at 4201°/s^2) and lowest with the Head Heavy racket (shoulder at 4905°/s^2 and elbow at 3710°/s^2). The Head Light racket also allows

for the most excellent range of motion, with the shoulder at 260.9° and the elbow at 120.2°, while the Head Heavy racket restricts the range of motion more, with the shoulder at 240.9° and the elbow at 111.3°.

Table 5. Kinematic patterns for different racket designs (Joint Angles, Velocities, Accelerations).

Kinematic Variable	Head Light	Even Balanced	Head Heavy
Maximal Shoulder Internal Rotation (°)	95.6 ± 3.5	90.1 ± 4.0	85.2 ± 4.2
Maximal Shoulder External Rotation (°)	165.3 ± 5.0	160.4 ± 4.6	155.7 ± 5.1
Maximal Elbow Flexion (°)	125.4 ± 3.2	122.6 ± 3.5	120.1 ± 3.9
Maximal Elbow Extension (°)	5.2 ± 1.0	7.0 ± 1.1	8.8 ± 1.2
Maximal Shoulder Angular Velocity (°/s)	1340.5 ± 105.8	1205.7 ± 115.2	1152.3 ± 121.5
Maximal Elbow Angular Velocity (°/s)	1012.4 ± 95.4	950.3 ± 90.8	890.2 ± 98.6
Maximal Shoulder Angular Acceleration (°/s^2)	5702 ± 650	5220 ± 590	4905 ± 670
Maximal Elbow Angular Acceleration (°/s^2)	4201 ± 520	3957 ± 510	3710 ± 580
Maximal Shoulder Range of Motion (°)	260.9 ± 10.4	250.5 ± 9.7	240.9 ± 11.0
Maximal Elbow Range of Motion (°)	120.2 ± 5.1	115.6 ± 4.8	111.3 ± 5.5

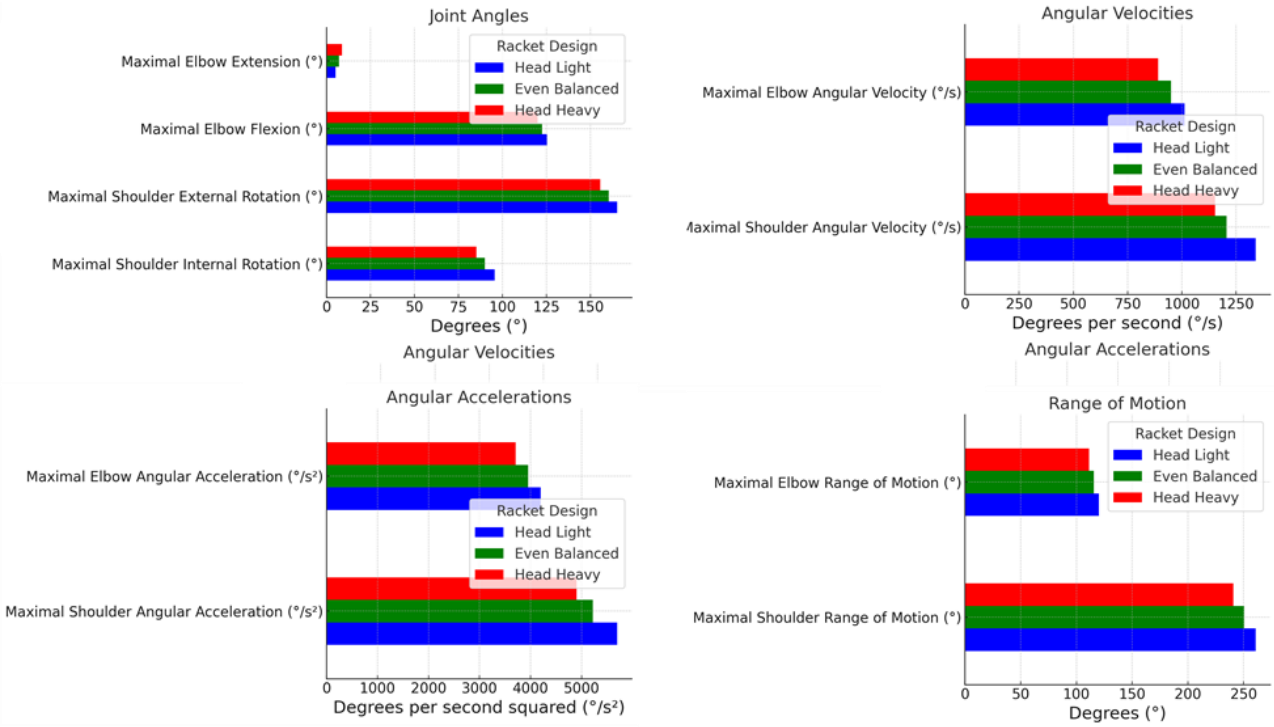

Figure 7. Kinematic result comparison for different racket designs.

The results from the Joint Power and Energy Transfer (**Table 6** and **Figure 8a)** demonstrate that the Head Light racket generates the highest joint power across all joints, with the shoulder producing 185.4 W, the elbow 142.3 W, and the wrist 105.2 W. In contrast, the Head Heavy racket shows the lowest power output, with the shoulder at 163.7 W, the elbow at 121.4 W, and the wrist at 92.1 W. The Even Balanced racket exhibits intermediate values, with the shoulder at 176.6 W, the elbow at 131.5 W, and the wrist at 98.7 W. These results suggest that lighter rackets allow for more efficient energy transfer, generating higher joint power output. The Moment-

to-Force Ratios results in **Table 7** and **Figure 8b** further reveal that the Head Heavy racket imposes the highest ratios, with the shoulder at 1.81 and the elbow at 1.63, indicating that a more significant proportion of the player's effort is required to control rotational forces. The Head Light racket shows the lowest ratios, with the shoulder at 1.36 and the elbow at 1.25, reflecting more efficient force application with less strain. The Even Balanced racket again demonstrates intermediate ratios, with the shoulder at 1.53 and the elbow at 1.47, balancing control and effort.

Table 6. Joint power and energy transfer for different racket Designs (Shoulder, Elbow, Wrist).

Racket Design	Joint Power (Shoulder) (W)	Joint Power (Elbow) (W)	Joint Power (Wrist) (W)
Head Light	185.4 ± 15.5	142.3 ± 12.8	105.2 ± 10.3
Even Balanced	176.6 ± 14.8	131.5 ± 11.9	98.7 ± 9.7
Head Heavy	163.7 ± 13.6	121.4 ± 10.5	92.1 ± 9.1

Table 7. Moment-to-force ratios for different racket designs (Elbow, Shoulder).

Racket Design	Moment-to-Force Ratio (Shoulder)	Moment-to-Force Ratio (Elbow)
Head Light	1.36 ± 0.10	1.25 ± 0.09
Even Balanced	1.53 ± 0.12	1.47 ± 0.11
Head Heavy	1.81 ± 0.15	1.63 ± 0.13

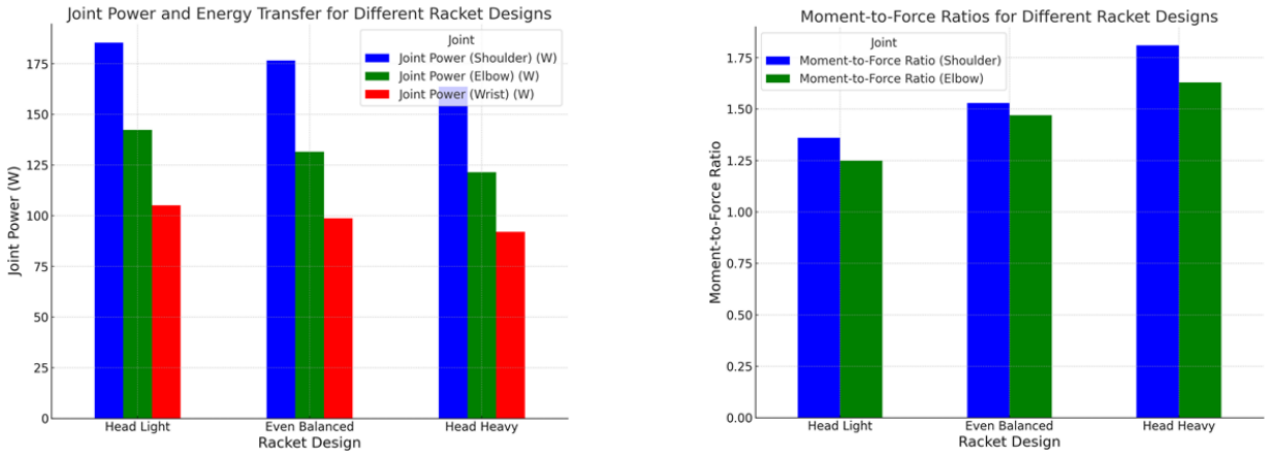

Figure 8. (a) Joint Power and Energy Transfer Analysis; **(b)** Moment-to-Force Ratio Analysis.

From the result (**Table 8 and Figure 9**) show clear trends across racket designs and serve speeds in the correlations between joint forces, moments, and ball speed. At all serve speeds, the Head Light racket has the highest correlations for shoulder, elbow, and wrist moments with ball speed. For instance, at 120–130 km/h, the shoulder moment correlation for the Head Light racket is 0.783, compared to 0.692 for the Even Balanced and 0.616 for the Head Heavy. The Head Heavy racket shows the lowest correlations across all speeds. Similarly, the Head Light racket has the strongest correlations for joint forces. At 120–130 km/h, the shoulder force correlation is 0.705 for the Head Light, compared to 0.641 for the Even Balanced and 0.559 for the Head Heavy. The wrist force follows the same pattern, with the Head Light showing 0.659, compared to 0.605 for the Even Balanced and 0.532 for the Head Heavy.

Table 8. Correlations between wrist force and ball speed at different serve speeds.

Serve Speed (km/h)	Shoulder Moment			Elbow Moment			Wrist Moment		
	Head Light	Even Balanced	Head Heavy	Head Light	Even Balanced	Head Heavy	Head Light	Even Balanced	Head Heavy
120–130 km/h	0.783	0.692	0.616	0.773	0.687	0.609	0.692	0.622	0.532
130–140 km/h	0.761	0.665	0.595	0.747	0.662	0.593	0.675	0.603	0.517
140–150 km/h	0.735	0.645	0.565	0.723	0.644	0.571	0.654	0.587	0.499
150–160 km/h	0.712	0.627	0.542	0.701	0.623	0.556	0.633	0.568	0.477
160+ km/h	0.688	0.598	0.515	0.678	0.602	0.527	0.611	0.549	0.455
Serve Speed (km/h)	**Shoulder Force**			**Elbow Force**			**Wrist Force**		
	Head Light	Even Balanced	Head Heavy	Head Light	Even Balanced	Head Heavy	Head Light	Even Balanced	Head Heavy
120–130 km/h	0.705	0.641	0.559	0.684	0.629	0.551	0.659	0.605	0.532
130–140 km/h	0.688	0.623	0.544	0.665	0.612	0.536	0.638	0.589	0.518
140–150 km/h	0.665	0.603	0.527	0.643	0.590	0.519	0.615	0.568	0.499
150–160 km/h	0.644	0.582	0.505	0.622	0.572	0.495	0.593	0.548	0.477
160+ km/h	0.621	0.560	0.483	0.600	0.553	0.472	0.571	0.527	0.455

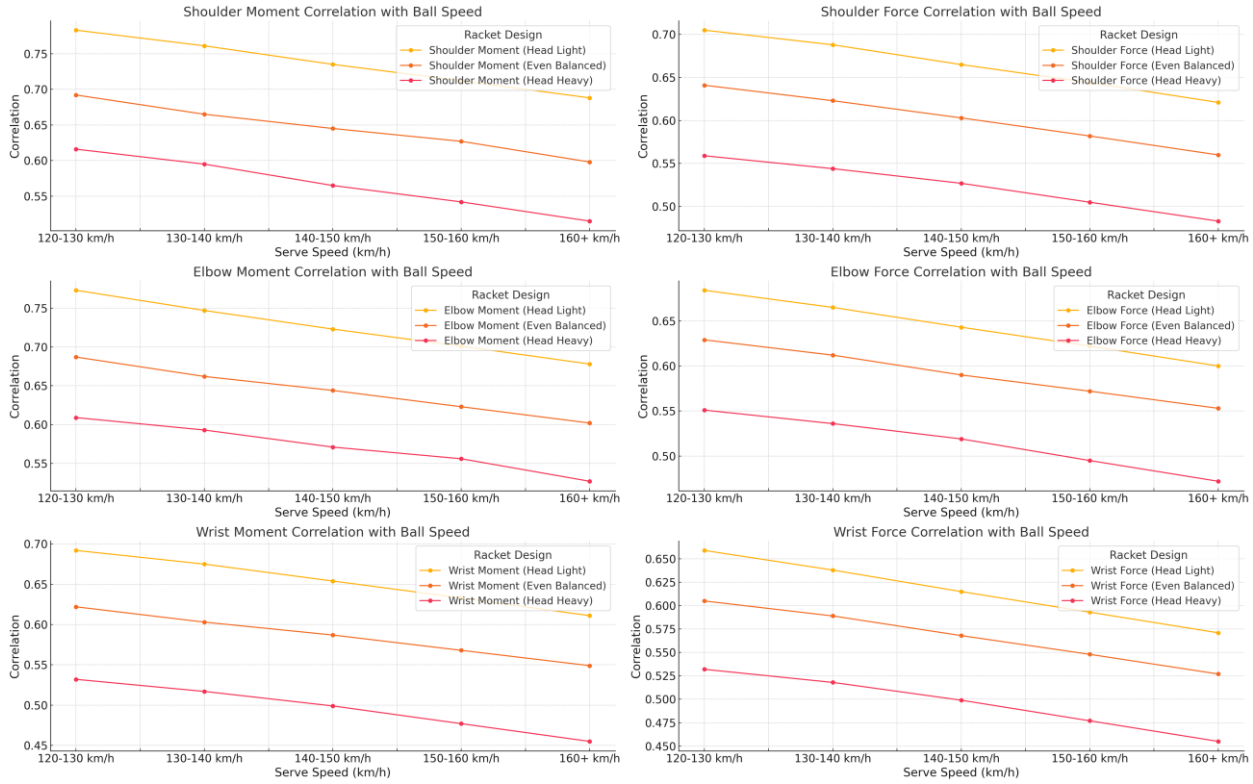

Figure 9. Correlation analysis between shoulder, elbow, and wrist against force and moment.

The cross-validation results for the LSTM model predictions of joint moments and forces, as depicted in **Table 9** and **Figure 10**, reveal that the Head Light racket consistently provides the best predictive performance across all metrics. For shoulder moments, the model shows the lowest Mean Absolute Error (MAE) of 2.315 Nm and Root Mean Square Error (RMSE) of 3.110 Nm, with an R^2 of 0.915, indicating substantial accuracy. In comparison, the Head Heavy racket has the highest errors,

with an MAE of 2.960 Nm, RMSE of 3.799 Nm, and the lowest R^2 of 0.876. For elbow moments, the Head Light racket again outperforms the other designs, with an MAE of 1.657 Nm and an R^2 of 0.930, while the Head Heavy racket produces the highest error values (MAE of 2.115 Nm and R^2 of 0.897). The pattern continues for wrist moments, where the Head Light racket achieves the best performance, with an MAE of 1.125 Nm, RMSE of 1.605 Nm, and R^2 of 0.942, while the Head Heavy racket lags with higher errors and an R^2 of 0.910. For joint forces, the Head Light racket again shows the best results. The shoulder force prediction yields an MAE of 25.672 N, RMSE of 32.855 N, and R^2 of 0.910. The Head Heavy racket has the highest errors, with an MAE of 32.569 N, RMSE of 39.523 N, and R^2 of 0.865. Similarly, for elbow and wrist forces, the Head Light racket consistently produces lower errors and higher R^2 values, while the Head Heavy racket results in the highest error values across these joints, reflecting more significant predictive discrepancies.

Table 9. Cross-Validation Results for LSTM Model Predictions of Joint Moments and Forces.

Joint	Metric	Head Light	Even Balanced	Head Heavy
Shoulder Moment	MAE (Nm)	2.315 ± 0.185	2.587 ± 0.210	2.960 ± 0.245
	RMSE (Nm)	3.110 ± 0.290	3.405 ± 0.315	3.799 ± 0.360
	R^2	0.915 ± 0.012	0.902 ± 0.015	0.876 ± 0.020
Elbow Moment	MAE (Nm)	1.657 ± 0.138	1.852 ± 0.150	2.115 ± 0.175
	RMSE (Nm)	2.220 ± 0.195	2.415 ± 0.205	2.711 ± 0.230
	R^2	0.930 ± 0.011	0.921 ± 0.013	0.897 ± 0.017
Wrist Moment	MAE (Nm)	1.125 ± 0.095	1.304 ± 0.102	1.498 ± 0.118
	RMSE (Nm)	1.605 ± 0.135	1.780 ± 0.145	2.003 ± 0.160
	R^2	0.942 ± 0.009	0.930 ± 0.011	0.910 ± 0.015
Shoulder Force	MAE (N)	25.672 ± 2.512	28.320 ± 2.715	32.569 ± 2.975
	RMSE (N)	32.855 ± 3.012	35.894 ± 3.325	39.523 ± 3.632
	R^2	0.910 ± 0.013	0.894 ± 0.015	0.865 ± 0.019
Elbow Force	MAE (N)	18.215 ± 1.810	21.275 ± 1.945	24.135 ± 2.180
	RMSE (N)	24.098 ± 2.115	26.510 ± 2.330	30.008 ± 2.640
	R^2	0.935 ± 0.010	0.920 ± 0.012	0.885 ± 0.017
Wrist Force	MAE (N)	12.103 ± 1.152	13.875 ± 1.245	15.495 ± 1.420
	RMSE (N)	17.520 ± 1.550	19.225 ± 1.655	21.490 ± 1.835
	R^2	0.947 ± 0.008	0.930 ± 0.010	0.905 ± 0.014

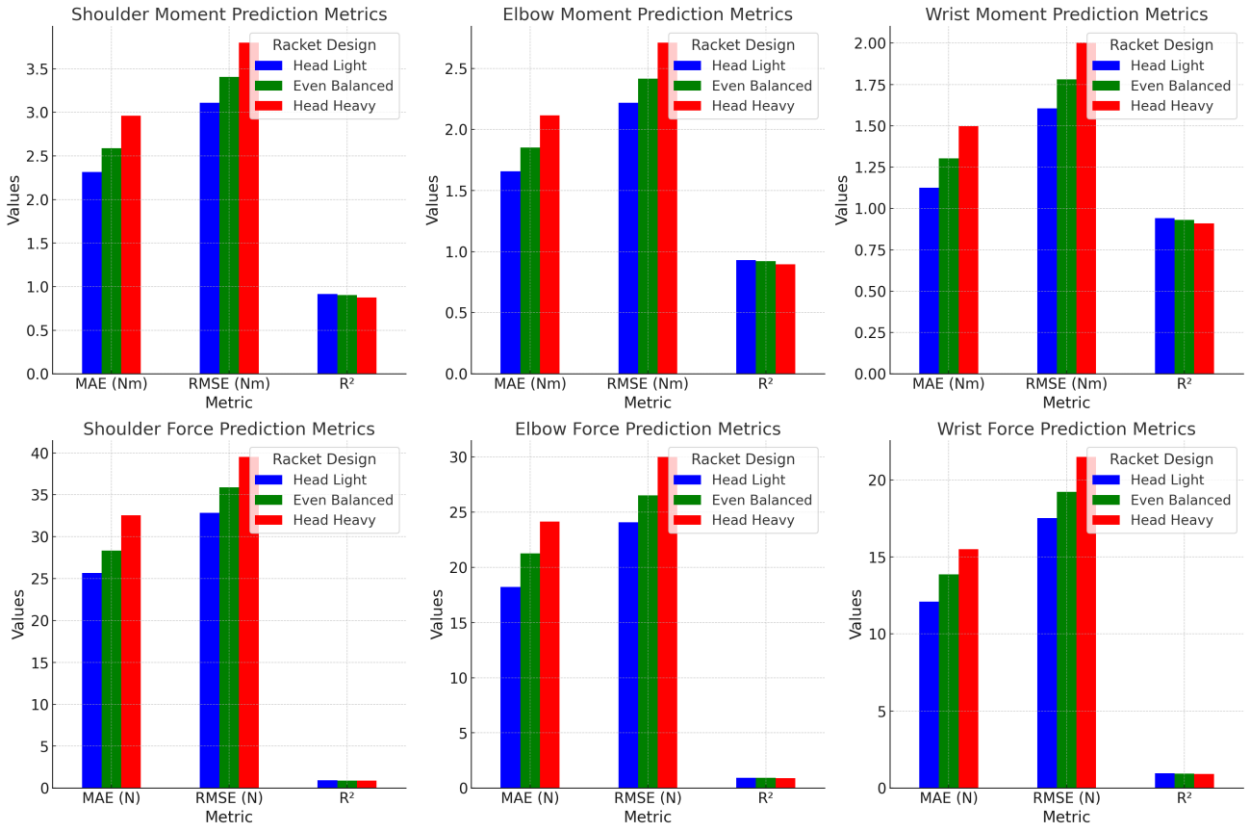

Figure 10. LSTM model performance analysis.

4. Conclusion and future work

This study explored the biomechanical effects of different racket designs, such as head-light, even-balanced, and head-heavy on shoulder, elbow, and wrist joint loading during tennis serves. The work employed eight players from the expert level and collected kinematic data, including joint angles, angular velocities, accelerations, and racket parameters captured during the three phases of the tennis serve. The data was then analyzed using the LSTM neural network model to predict joint moments and forces. The study investigated how varying racket characteristics influence joint mechanics across the different phases of a serve. From the results, it can be ascertained that racket design plays a key role in determining the mechanical loads experienced by the upper limb joints. The findings show that the head-light racket reduces joint moments and forces in both the shoulder and elbow during the acceleration phase of the serve. This racket type had achieved a shoulder adduction moment of 9.4 ± 0.8 Nm and a shoulder force of 130.2 ± 9.4 N. The head-heavy racket produced a higher shoulder adduction moment of 11.3 ± 1.0 Nm and a force of 162.3 ± 11.4 N, and the even-balanced racket showed intermediate values. The results suggest that the head-light racket is better in terms of minimal joint stress and better performance.

Future work would investigate the long-term impacts of racket design on joint health and explore larger participant groups to generalize the findings.

Author contributions: Conceptualization, QM and HZ; methodology, QM and HZ; software, QM and HZ; validation, QM and HZ; formal analysis, QM and HZ; investigation, QM and HZ; resources, QM and HZ; data curation, QM and GZ;

writing—original draft preparation, QM and HZ; writing—review and editing, QM and HZ; visualization, QM and HZ; supervision, QM and HZ; project administration, QM and HZ; funding acquisition: QM and HZ**.** All authors have read and agreed to the published version of the manuscript.

Ethical approval: Not applicable.

Conflict of interest: The authors declare no conflict of interest.

References

1. Mulya G, Lengkana AS, Agustryani R. TennBasTech: A Scientific Approach to Teach Tennis. International Journal of Human Movement and Sports Sciences. 2021; 9(6): 1371-1382. doi: 10.13189/saj.2021.090633
2. Israel JS, Loushin SR, Tetzloff SU, et al. Wrist Motion Assessment in Tennis Players using Three-Dimensional Motion Capture and Dynamic Electromyography. Journal of Wrist Surgery. 2023; 13(03): 264-271. doi: 10.1055/s-0043-1777024
3. Patel J, Wallen M. Four Common Upper Body Injuries in Tennis Players: Prevention, Description, and Treatment. Academic Medicine & Surgery. Published online May 1, 2024. doi: 10.62186/001c.117284
4. Oyama S, Prentice WE. Rehabilitation of Elbow Injuries. Rehabilitation Techniques for Sports Medicine and Athletic Training. Published online May 28, 2024: 507-536. doi: 10.4324/9781003526308-22
5. Hibberd E, Myers JB, Pexa B, et al. Rehabilitation of Shoulder Injuries. Rehabilitation Techniques for Sports Medicine and Athletic Training. Published online May 28, 2024: 435-506. doi: 10.4324/9781003526308-21
6. Cádiz Gallardo MP, Pradas de la Fuente F, Moreno-Azze A, et al. Physiological demands of racket sports: a systematic review. Frontiers in Psychology. 2023; 14. doi: 10.3389/fpsyg.2023.1149295
7. Liu S, Wu C, Xiao S, et al. Optimizing young tennis players' development: Exploring the impact of emerging technologies on training effectiveness and technical skills acquisition. Gu Y, ed. PLOS ONE. 2024; 19(8): e0307882. doi: 10.1371/journal.pone.0307882
8. Goislard de Monsabert B, Herbaut A, Cartier T, et al. Electromyography-informed musculoskeletal modeling provides new insight into hand tendon forces during tennis forehand. Scandinavian Journal of Medicine & Science in Sports. 2023; 33(10): 1958-1975. doi: 10.1111/sms.14434
9. Ma X, Yaacob A, Kamalden TFT, & NG YG. To Assess the Impact of Physical Factors on Velocity, Speed, and Accuracy of Tennis Serve. Journal of Natural Science, Biology and Medicine. 2024; 15(1): 125.
10. Edriss S, Romagnoli C, Caprioli L, et al. The Role of Emergent Technologies in the Dynamic and Kinematic Assessment of Human Movement in Sport and Clinical Applications. Applied Sciences. 2024; 14(3): 1012. doi: 10.3390/app14031012
11. De Luigi AJ. The effects on sports performance of technologic advances in sports prostheses and wheelchairs. PM&R. 2024; 16(4): 409-417. doi: 10.1002/pmrj.13153
12. Suwannachote N, Imjai T, Wattanapanich C, et al. Experimental and Computer Simulation Studies on Badminton Racquet Strings. Sensors. 2023; 23(13): 5957. doi: 10.3390/s23135957
13. Berhimpong MW, Mangolo EW, Makadada FA, et al. Exploring the impact of drills training and grip strength on tennis serve performance: A factorial experimental design research. Journal of Physical Education and Sport. 2023; 23(11): 3108-3118.
14. Irawan R, Azam M, Rahayu S, et al. Biomechanical Motion of the Tennis Forehand Stroke: Analyzing the Impact on the Ball Speed Using Biofor Analysis Software. Physical Education Theory and Methodology. 2023; 23(6): 918-924. doi: 10.17309/tmfv.2023.6.14
15. Touzard P, Lecomte C, Bideau B, et al. There is no rush to upgrade the tennis racket in young intermediate competitive players: The effects of scaling racket on serve biomechanics and performance. Frontiers in Psychology. 2023; 14. doi: 10.3389/fpsyg.2023.1104146
16. Liu A, Lin YT, Sundaresan K. View-agnostic Human Exercise Cataloging with Single MmWave Radar. Proceedings of the ACM on Interactive, Mobile, Wearable and Ubiquitous Technologies. 2024; 8(3): 1-23. doi: 10.1145/3678512
17. Yu H, Tu J, Wang P, et al. Bat Planner: Aggressive Flying Ball Player. IEEE Robotics and Automation Letters. 2023; 8(9): 5307-5314. doi: 10.1109/lra.2023.3293355

18. Allen T, Choppin S, Knudson D. A review of tennis racket performance parameters. Sports Engineering. 2015; 19(1): 1-11. doi: 10.1007/s12283-014-0167-x
19. Patel H, Lala S, Helfner B, et al. Tennis overuse injuries in the upper extremity. Skeletal Radiology. 2020; 50(4): 629-644. doi: 10.1007/s00256-020-03634-2
20. Gordon BJ, Dapena J. Contributions of joint rotations to racquet speed in the tennis serve. Journal of Sports Sciences. 2006; 24(1): 31-49. doi: 10.1080/02640410400022045
21. Colomar J, Corbi F, Brich Q, et al. Determinant Physical Factors of Tennis Serve Velocity: A Brief Review. International Journal of Sports Physiology and Performance. 2022; 17(8): 1159-1169. doi: 10.1123/ijspp.2022-0091
22. Fett J, Ulbricht A, Ferrauti A. Impact of Physical Performance and Anthropometric Characteristics on Serve Velocity in Elite Junior Tennis Players. Journal of Strength and Conditioning Research. 2020; 34(1): 192-202. doi: 10.1519/jsc.0000000000002641
23. Hayes MJ, Spits DR, Watts DG, et al. Relationship Between Tennis Serve Velocity and Select Performance Measures. Journal of Strength and Conditioning Research. 2021; 35(1): 190-197. doi: 10.1519/jsc.0000000000002440
24. Cant O. Exploring the effects of ball speed and spin in Grand Slam tennis match-play [PhD thesis]. Victoria University; 2020.
25. Jacquier-Bret J, Gorce P. Kinematics characteristics of key point of interest during tennis serve among tennis players: A systematic review and meta-analysis. Frontiers in Sports and Active Living. 2024; 6. doi: 10.3389/fspor.2024.1432030
26. Antúnez R, Hernández F, García J, et al. Relationship Between Motor Variability, Accuracy, and Ball Speed in the Tennis Serve. Journal of Human Kinetics. 2012; 33(2012): 45-53. doi: 10.2478/v10078-012-0043-3
27. Lo KC, Hsieh YC. Comparison of ball-and-racket impact force in two-handed backhand stroke stances for different-skill-level tennis players. Journal of sports science & medicine. 2016; 15(2): 301.
28. Knudson D, Allen T, Choppin S. Interaction of Tennis Racket Design and Biomechanical Factors. Routledge Handbook of Ergonomics in Sport and Exercise. 2013: 423-435. doi: 10.4324/9780203123355-43